Accurate Evaluation of Antenna Measurement Range Performance with the SWE Transmission Formula

Francesco Saccardi, *AMTA Senior,* Andrea Giacomini, *AMTA Senior,*
Lars J. Foged, *AMTA Fellow*
Microwave Vision Italy SRL, Via dei Castelli Romani 59, 00071, Pomezia, Italy
francesco.saccardi@mvg-world.com

***Abstract*—The spherical wave expansion-based transmission formula allows to accurately evaluate the coupling (or S_{21} parameter) between a transmitting and a receiving antenna. Its use as tool for probe corrected spherical near-field to far-field transformation is well accepted and documented. On the other hand, its direct use in the evaluation of antenna measurement performance has been exploited only in recent years. In this paper we will show how measurement performances predicted with the transmission formula compare with actual measurements. Taking as examples relatively complex antenna measurement systems like spherical near-field, plane wave generators and CATR, we will focus on the prediction of the accuracy of the measured radiation patterns, also including the approximation of reflections from the test environments, and on the evaluation of link budgets.**

I. Introduction

Accurate emulations of antenna measurements are essential to predict the performance of measurement ranges and evaluate their uncertainty. Typical antenna test systems are based on the measurements of the coupling between a transmitting (or receiving) Antenna/Device Under Test (AUT/DUT) and a receiving (or transmitting) device such as probes, range antennas, CATR or Plane Wave Generators (PWG). Such coupling measurements can be efficiently and accurately emulated with the well-known Spherical Wave Expansion (SWE)-based Transmission Formula (TXF). As widely described in [1], from the spherical wave spectrum of both the TX and RX antennas, their direct coupling (i.e. the S_{21} parameter) can be evaluated in any point in space as long as the minimum spheres of the two antennas do not intersect [1]. While the transmission formula is a standard tool for probe corrected spherical near-field to far-field (NF/FF) transformation [2], its direct use in the evaluation of antenna measurement performance has been exploited only in recent years [3]-[4].

A typical example is the evaluation of the probe influence in Spherical Near Field (SNF) measurements. Similarly, measurement performances of more complex CATR and PWG systems can also effectively be evaluated with the TXF. Such devices create a plane wave in a region called quiet zone (QZ) located in the NF of the CATR or PWG. Performances of such systems are normally expressed in terms of field uniformity in the QZ which hardly translate to direct contributions of an antenna measurement uncertainty analysis. Instead, actual CATR/PWG-based antenna measurements can be emulated with the transmission formula allowing a direct evaluation of the measurement accuracy [4].

The estimation of the measurement dynamic range is another important aspect during the design of an antenna measurement range. While in FF ranges this can easily be treated with the well-known Friis' formula [5], in NF and CATR/PWG systems it becomes more critical because of the "NF-effect" introduced by the reduced distance and the measurement device (e.g. probe, CATR reflector, PWG etc..). Considering gain-calibrated spherical wave spectra of both the TX and RX devices, the transmission formula can also be exploited to evaluate the actual signal level in test regions located at any distance (outside the minimum sphere) and hence to properly estimate the dynamic range of any antenna measurement system [6].

Given all these valuable usages of the TXF, in this paper we will show for the first time how its predictions compare to actual measurements performed in the same conditions or with calculations performed with other techniques.

II. The SWE-Based Transmission Formula

The transmission formula (TXF) is reported in equations (1) and (2) below.

$$w(r,\chi,\theta,\varphi) = \sum_{\substack{smn \\ \mu}} Q^{(4)}_{smn} e^{jm\varphi} d^{n}_{\mu m}(\theta) e^{j\mu\chi} P^{(4)}_{s\mu n}(kr) \qquad (1)$$

$$P^{(4)}_{s\mu n}(kr) = \sum_{\sigma\nu} C^{sn(4)}_{\sigma\mu\nu}(kr) R^{p}_{\sigma\mu\nu} \qquad (2)$$

Such formula expresses the complex signal received by a probe (w) of known Spherical Wave Coefficients (SWC, $R^{p}_{\sigma\mu\nu}$) as a function of the probes coordinates (r,θ,φ) and orientation (χ) when an AUT/DUT described by its own SWC ($Q^{(4)}_{smn}$) transmits. The symbols $d^{n}_{\mu m}(\theta)$ and $C^{sn(4)}_{\sigma\mu\nu}(kA)$ are respectively rotation and translation operators that, together with the two complex exponentials ($e^{jm\varphi}$ and $e^{j\mu\chi}$), are used to describe the probe position/orientation in each measurement point. The quantity $P^{(4)}_{s\mu n}(kr)$ is called probe response constant and is traditionally written in a separated term because it only depends on the probe SWC, the measurement distance and the frequency.

Probe correction in SNF measurements is the most widespread application of the TXF [1],[7],[8]. In such cases the TXF is inverted by mean of the SWC of the DUT exploiting the measured signal $w(r,\chi,\theta,\varphi)$ and the probe SWC. Direct application of the TXF is normally employed to compute the FF

radiation pattern from the SWC of the DUT. The TXF is also a very powerful and accurate tool for the evaluation/prediction of antenna measurement range performance. The only limitation of the TXF is that the coupling signal must be computed at sufficiently large distance so that the DUT and probe minimum sphere do not intersect [1]. Moreover, the TXF as reported above, only allows the computation of the direct coupling. The computation of the mutual coupling will not be treated in this paper. Interested readers can refer to the scattering matrix theory detailed in [1].

III. Evaluation of Antenna Range Performance

In this section we focus of the prediction of the antenna range performance by using the TXF. Examples of emulation of NF pattern measurements including the effect of generic probes and reflections from the measurement environment will be provided. Similarly, examples of Quiet Zone (QZ) probing with different measurement devices will also be shown.

A. Antenna Pattern Measurement Emulation

We consider the SNF measurement setup shown in Figure 1. The AUT is the X-band Standard Gain Horn (SGH820) mounted on a robotic-arm, used to perform the roll/azimuth (or φ/θ) scanning. The probe is the open-boundary quad-ridge horn (MVG QH800) mounted on the tower on the right side. As already pointed out in [7], such a probe has a high radial and azimuthal modal content, generating a complex (e.g. asymmetric sidelobes and cx-polar) and relatively highly directive pattern (approx. 15dBi).

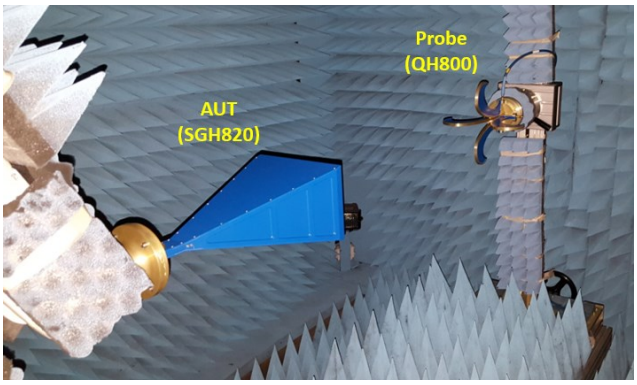

Figure 1. Robotic-arm based SNF range setup.

The blue solid/dashed traces in Figure 2. are the co-polar/cx-polar normalized E-plane pattern at 10GHz, measured at 1.2m distance. From the full-wave simulated model of both SGH820 and the QH800, the TXF has been applied to emulate the same SNF measurement. The obtained SNF pattern along the same cut is shown by the orange traces in Figure 2. The agreement with the real measurement is very good, both for the co-polar and cx-polar pattern. The black trace in the same figure illustrates the SNF emulation of the SGH820 with an ideal Hertzian dipole. Significant differences on the sidelobes and cx-polar are observed.

The good agreement between the measured and the emulated pattern with the TXF, allows to appreciate the accuracy of this measurement emulation approach for the evaluation of the antenna range performance. Emulations like this one for example, allow to evaluate the effect of the measurement probe when different post-processing are applied (e.g. NF/FF w/o probe correction, with first order probe correction etc..).

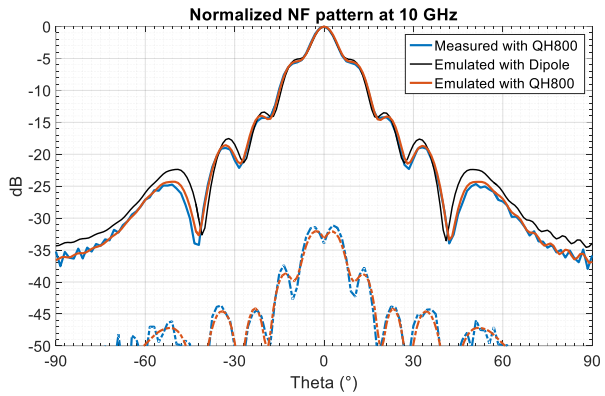

Figure 2. Comparison bewteen measured and emulated NF patterns at 1.2m with the TXF. Co-polar (solid) and cx-polar (dashed) E-plane pattern.

B. Anechoic Chamber Effect Emulation

Another important aspect of the evaluation of the antenna range performance is the effect of the measurement environment, which could generate unwanted reflections. A relatively simple approach based on the combination of the SWE-based TXF and image-theory has already been reported in [3] and will only be recalled here.

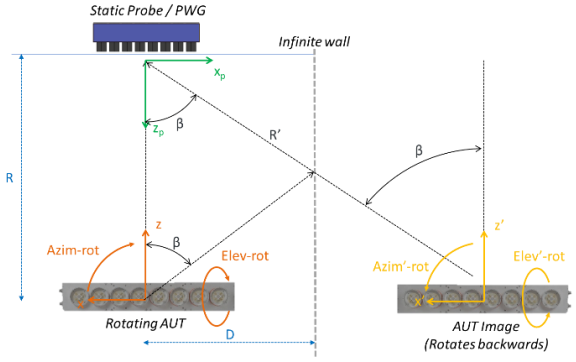

Figure 3. Schematic of the SWE/Image-based method to evaluate the reflection effect.

Let us consider the measurement scenario shown in Figure 3. , where a PWG is used to illuminate an AUT mounted on a two-axis positioner (elevation-over-azimuth in this case). Rotations of the AUT that replicate the same actual movement of the device during the scanning can be applied on the (known) SWC of the AUT [1]. For each AUT position, the TXF is applied considering the (known) SWC of PWG. As also described in [4], this allows to directly evaluate the quality of the plane wave generated by the PWG with an emulation of a realistic antenna measurement scenario. Consequently, the derivation of certain contributions to the measurement uncertainty is much easier than an analysis based on the variation of the field in the QZ (i.e. QZ probing).

To also include the residual effect of the walls of the anechoic chamber, the image of the of the AUT can be considered as shown in Figure 3. Without loss of generality, the image due to the right wall is shown. Such an image rotates backward, with respect to the AUT. For each position of the image, the coupling with the PWG is evaluated again with the TXF. Of course, in this case the SWC of the PWG must be properly counter rotated to account for the displaced position of the image. Once this "image-PWG" coupling is computed, it is weighted according the absorption properties of the materials on the wall, which depends on the incident angle (β). This process is then repeated for each wall/ceiling/floor, and finally all the computed contributions are superposed.

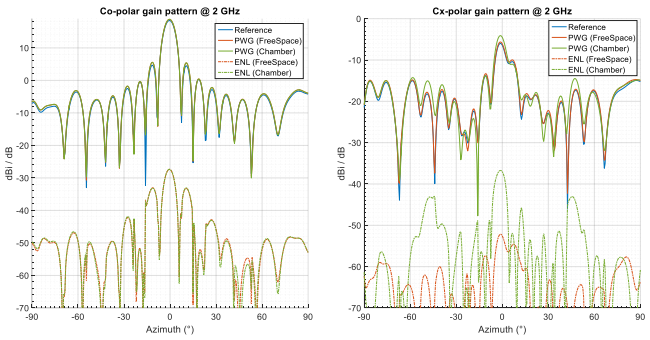

Figure 4. Emulated gain pattern measurement of a base-station antenna at 2 GHz performed with the PWG.

Figure 4. shows an example of this method [3]. The considered PWG works in the 1.4-5.5 GHz frequency range and generates a 1.5m-diameter spherical QZ at 3.3 m from its aperture. The AUT is a slant-45 polarized base-station antenna at 2 GHz. The SWC of such an AUT have been obtained from real measurements. The modelled anechoic chamber has a rectangular footprint and is covered with 12-inch absorbers with -37 dB reflectivity at normal incidence. The emulated co-polar and cx-polar gain patterns (solid traces) are shown in Figure 4. for the free-space (red traces) and chamber scenarios (green traces). The pointwise Equivalent Noise Level (ENL) computed as weighed difference between the emulated measurement and the reference pattern is also shown (dashed traces). The chamber effect on the measured co-polar pattern is negligible (global RMS ENL is approx. -40 dB in both cases). The chamber has more impact on the cx-polar pattern where the global ENL increase from -61 dB (free-space) to -48 dB.

C. Quiet Zone Probing Emulation

The amplitude/phase uniformity of the QZ of a PWG, a CATR or a simple direct FF system is usually the main metric during the design stages of such systems. Emulating a QZ probing with realistic probes is also often needed because it allows fair comparisons of predicted and actual measured data. This can be performed with the TXF by considering the SWC of the radiating device (e.g. PWG, CATR or range antenna) and the SWC of the measuring probe. Since QZ field are usually expressed in terms of a cartesian grid, the "native" spherical coordinates $w(r,\chi,\theta,\varphi)$, normally used in the SWE-based TXF, must be properly converted to xyz-cordinates. Moreover, for each sampling position the probe SWC must be counter rotated to maintain the alignment with the boresight of the measurement system.

It is pointed out that, like in the previous situation, the chamber effect can also be included in the QZ probing emulation with the same SWE/image-theory based approach.

As an example, we consider a 10-40 GHz direct FF system with a closed boundary quad-ridge horn (QR18000) as range antenna. The spherical QZ is centered at 6m and has a diameter of 1m. From the SWC of the QR18000 at 30GHz, the down-range QZ probing has been emulated in different conditions. The four maps of Figure 5. are the emulated probing with/without the chamber effect (4 x 7.5m chamber with -50dB wall reflectivity) and considering an ideal Hertzian dipole as probe (top) or a realistic probe, the QH4000 open-boundary quad-ridge horn, with approx. 16dBi directivity (bottom). The free-space emulations (left column) are useful to evaluate the taper introduced by the range antenna at such measurement distance. As expected, the real probe increases the taper giving rise to an overestimation of this quantity. This is due to the field integration over the probe aperture (i.e. spatial convolution). The emulation of chamber effect (right column) allows to estimate the QZ ripple. In this case, less ripple is observed when the QH4000 is used. This is due to the same field integration on the probe aperture, and the filtering effect of the probe pattern which attenuates the reflected signals from the chamber walls [9]. It is remarked that such types of emulations are very useful to better correlate predicted and measured QZ performances.

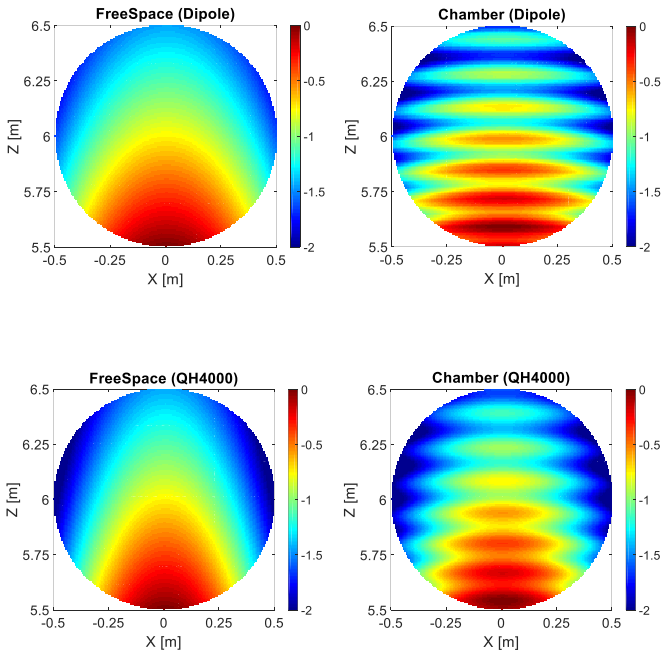

Figure 5. Example of QZ probing emulation with/without chamber effect, and with ideal dipole or realistic probe. Downrange of a FF system at 30GHz

IV. Link Budget Evaluation

The evaluation of the dynamic range of any antenna measurement system is of primarily importance. Accurate prediction of the link budget between the transmitting and receiving device is hence needed in the design stages of an antenna measurement system.

The link budget of direct FF systems can be evaluated in a very straightforward way with the well-known Friis' formula [5], which allows to compute the coupling between two antennas from the knowledge of their realized gain, the Free Space Path Loss (FSPL) and the conducted loss.

On the other hand, in case of antenna ranges operating at reduced distance, the Friis' formula cannot be used because the FF conditions are not met. NF, PWG and CATR systems fall in this category. In such cases, the SWE-based TXF can be used instead. Indeed, by using gain-normalized SWC [1] of the both transmitting and receiving devices, the TXF becomes a generalization of the Friis' formula usable at any measurement distance larger than the sum of the minimum sphere radius of the TX and RX devices. Examples of link budget computations with the SWE-based TXF for different antenna measurement systems are provided here in sub-section A.

Another way to extend the use of the Friis' formula to measurement scenarios with reduced measurement distances, is to define a quantity called NF directivity, which takes into account for the radiation pattern deformation due to the shorter distance. A description of this approach along with an example will be reported in sub-section B.

A. Examples of link budget calculation with TXF

In this sub-section, three examples of link budget evaluation for antenna measurement systems operating at short distance (a SNF range, a CATR and a PWG) will be reported.

1) Spherical NF range example

The SNF measurement scenario already shown in Figure 1. is again considered. The S_{21} parameter in the boresight direction has been measured by calibrating the system at the ports of the transmitting/receiving devices (SGH820 and QH800 respectively). The measured S_{21} over frequency is the trace with blue markers in Figure 6. The same S_{21} has been emulated with the TXF considering the gain-normalized SWC of the antennas, both obtained from full-wave simulations. The computed values are also reported in Figure 6. (See trace with orange markers). The agreement with the measured data is excellent. The 0.8dB maximum deviation at 10.5GHz is within the uncertainty of the modelled losses of both the considered antennas.

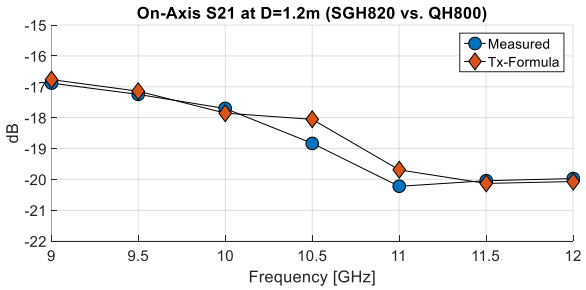

Figure 6. Comparison between measured and emulated on-axis S21 parameter in the SNF setup.

2) CATR example

As a second example, let us consider a relatively large CATR nominally working from 400MHz. The dimension of the rolled-edge reflector is approx. 13x11m and the focal distance is about 19m. The QZ is centered at 25m from the center of the reflector.

The link budget of a CATR system is normally calculated considering the Friis' FF formula in the feed-to-reflector region, hence knowing the gain of the feed and assuming the feed-to-reflector distance is sufficiently large to meet the FF criteria for the feed. 0dB FSPL are then considered in the reflector-to-QZ region, assuming that the reflected field is collimated on a flux of energy without losses. This approach is widely accepted in case of "well-designed" CATR systems [10].

The link budget of this CATR has been calculated starting from 100MHz, a much lower frequency than the nominal one (400MHz). The calculation with the conventional Friis' formula in the feed-to-reflector region is illustrated by the trace with blue markers in Figure 7. The computation with the SWE-based TXF, applied considering the SWC of CATR system obtained from full-wave simulation, is instead illustrated by the trace with orange markers. In both cases, an ideal Hertzian dipole has been assumed as receiving device in the center of the QZ. As can be seen, almost identical evaluation of the S_{21} parameters have been computed with the two methods at 300, 400 and 500MHz. More than 2dB deviations are instead obtained 100 and 200MHz, being outside the design frequency of such a CATR. Indeed, at such low frequencies, the system is not able to transform the spherical wave radiated by the feed, to a constant flux of energy. Consequently, the use of the conventional Friis' formula is much less accurate at such frequencies because the required assumptions are not anymore valid.

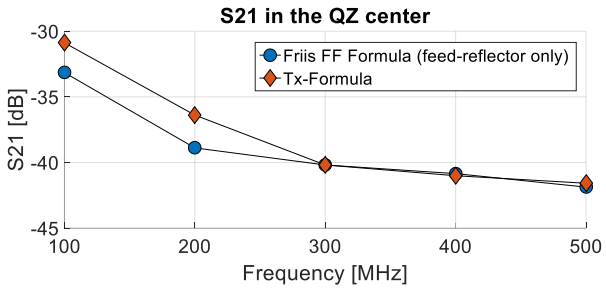

Figure 7. S21 parameter in the QZ center of a low-frequency CATR. Calculated with Friss FF formula and emulated with the TXF.

3) PWG example

Let's now consider the Plane Wave Generator (PWG) array working in the range 0.6 – 6GHz [11] shown in Figure 8. A PWG is an array with suitable lattice and complex excitation coefficients able to generate a spherical QZ at relatively close distance. Like in a CATR, the QZ is on the NF region of the PWG, hence the conventional FF Friis' formula cannot be used to evaluate the link budget. In this example we will show how the SWE-based TXF allows to accurately evaluate the link budget of such type of systems.

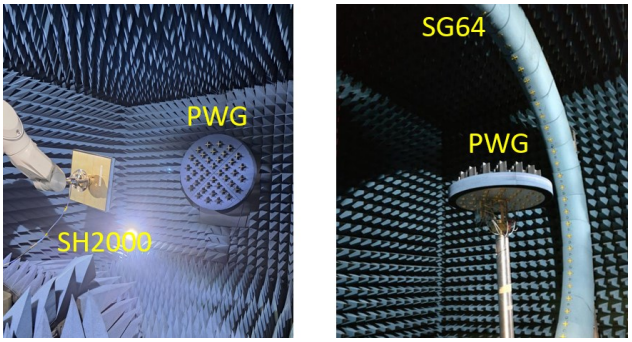

Figure 8. Sub-6GHz PWG. Measurement setup used to directly measure the S21 in the QZ center (left). Multiprobe SNF measurement setup (right).

One of the advantages of an array-based PWG is its reconfigurability. Its complex coefficients can in fact be chosen arbitrarily to achieve the desired trade-off between QZ uniformity and power density available in the QZ (e.g. usually the QZ uniformity is improved at the expense of energy available in the QZ and vice-versa).

The considered sub-6GHz PWG has been installed in the anechoic chamber shown on the left side of Figure 8. Three sets of complex excitation coefficients have been defined. For each configuration, the on-axis S_{21} parameter has been measured in the 3-6GHz frequency range with a dual-ridge horn antenna (the MVG SH2000) mounted on a robotic-arm at 1.7m distance. The measurements have been performed with a VNA calibrating the RF chain at the input ports of the PWG and of the SH2000 respectively. The three measured S_{21} parameters are reported in Figure 9. (see solid traces). The first set of coefficients (blue trace) maximizes the power in the QZ but provides worse QZ performances. Conversely, the third set of coefficients, minimize the field variation inside the QZ but provides a reduced signal power level.

To validate the TXF for such a type of systems, the same direct-coupling measurements have been emulated starting from the gain-normalized SWC of the PWG and the SH2000. The latter have been obtained from full-wave simulation. The SWC of the PWG have been obtained from gain calibrated SNF measurements performed in the SG64 multi-probe systems, as shown on the right side of Figure 8. More specifically, each individual sub-array of the PWG has been measured in an embedded configuration, and then the measured data have superposed with the same complex excitation coefficients previously considered. The emulated couplings with the TXF are compared in Figure 9 to the real S_{21} measurements. The agreement between real measurements and emulation is good. It is highlighted, that some PWG components have been replaced in the direct-S_{21} and SG64 measurement scenarios. This change, together with the uncertainties of both the involved measurements systems explains some larger deviations observable at some frequencies.

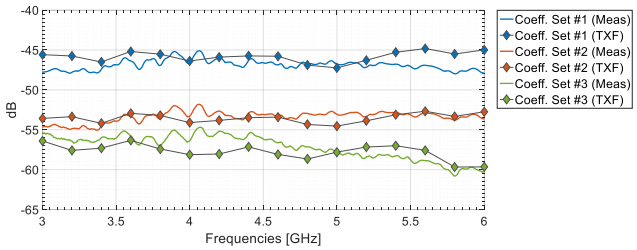

Figure 9. Sub-6GHz PWG. Comparison between measured and emulated S21 parameter in the QZ center, for different array exitation coefficients.

B. Near Field Directivity and Gain

We present here and alternative and straightforward way to evaluate the link budget of antenna measurement systems operating in the NF region of either the AUT and/or the measurement device. The idea is to generalize the Friis' formula, considering a modified version of the gain of the transmitting or receiving device to take into account the deformation of the radiation pattern, due to the reduced measurement distance.

In equation (3) the NF directivity, $D_{NF}(r,\theta,\varphi)$, of a generic radiating device is defined:

$$D_{NF}(r,\theta,\varphi) = 4\pi \frac{w_t(r,\theta,\varphi)^2}{\int_{\varphi=0}^{2\pi}\int_{\theta=0}^{\pi} w_t(r,\theta,\varphi)^2 \sin\theta \, d\theta d\varphi} \quad (3)$$

Such a quantity is obtained from $w_t(r,\theta,\varphi)^2 = \left[|w_\theta(\theta,\varphi)|^2 + |w_\varphi(\theta,\varphi)|^2\right]$, which is the radiation pattern at a generic distance r, from the origin of the coordinate system. When r is sufficiently large, the conventional distance-independent definition of directivity is obtained.

The NF gain, $G_{NF}(r,\theta,\varphi)$, can then be defined as $G_{NF}(r,\theta,\varphi) = \eta D_{NF}(r,\theta,\varphi)$ considering the efficiency of the radiating device (η).

Considering an electrically small receiving device, the Friis' formula is extended to measurement systems operating in the NF region as follow:

$$S_{21}(r,\theta,\varphi) = \frac{G_{NF,TX}(r,\theta,\varphi) G_{RX}(\theta,\varphi)}{FSPL(r,f)} \quad (4)$$

where the $FSPL(r,f) = (4\pi rf/c)^2 (4\pi rf/c)^2$ are the free space path loss defined in the conventional way.

To validate this alternative approach, we consider a low frequency PWG with starting frequency f_0. Such a device has a

diameter of approx. 4.5λ at f_0, and generates a spherical QZ of 1.5λ at 6.3λ distance. Figure 10. (left) illustrates the down-range S_{21}-map of such a PWG computed with the SWE-based TXF, considering an ideal (lossless) beam forming network of the PWG and an Hertzian dipole as receiving device. The QZ can clearly been identified at about 6.3λ distance. Figure 10. (right) illustrate the S_{21} at different frequencies, for the three locations inside the QZ (D_1, D_2, D_3). The three traces are almost identical, remarking the good field uniformity inside the QZ.

The S_{21} in the same three locations inside the QZ have been evaluated with the presented alternative method and reported on the right side of Figure 11. As can been seen, such achieved results are basically identical to those obtained with the TXF.

To gain insights on this alternative approach, we consider the NF directivity patterns of the PWG, evaluated at the three distances inside the QZ (D_1, D_2, D_3), and, for only comparative purposes, at infinite FF distance. In the boresight direction, the NF directivity at f_0 gradually increases from approx. 10dBi to 12.5dBi when increasing the distances inside the QZ. Such variation is compensated by the inverse of the FSPL which decreases of the same factor, giving rise to the (almost) constant field inside the QZ.

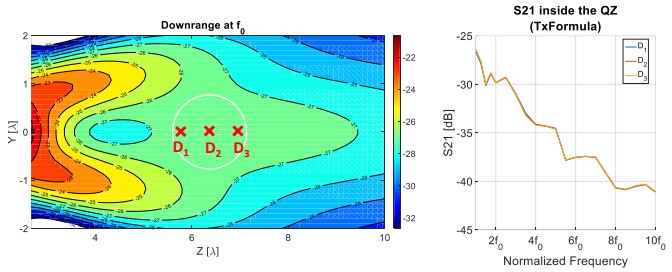

Figure 10. Low frequency PWG: Downrange S21-colormap at f0 (left); S_{21} parameter vs frequency emulated with the tx-formula in three different positions in the QZ.

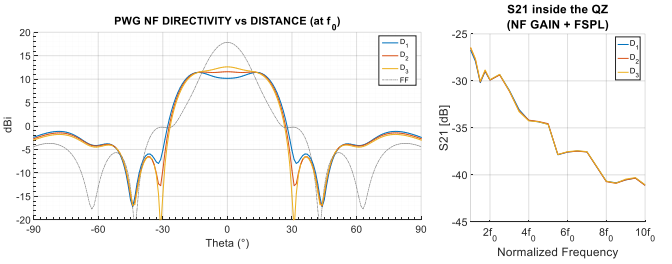

Figure 11. Low frequency PWG: NF directivity pattern at different distance (left); S_{21} parameter vs frequency calculated from the NF gain/directivity and the FSPL in three different positions in the QZ.

V. Conclusions

In this paper the spherical wave expansion-based transmission formula has been presented as a powerful tool for the prediction of the antenna range measurement performance. The transmission formula allows to accurately compute the complex coupling between a transmitting and a receiving device from the knowledge of their spherical wave spectra. Rota-translation of the spectrum of the devices allows the emulation of a variety of scanning schemes including the effect of possible reflections from the measurement environment.

Different examples to show the accuracy of the transmission formula in the prediction of the effect of the measurement device, like a NF probe, a PWG or CATR reflector, have been reported. Moreover, considering similar examples, it has been shown how the transmission formula can be used to accurately compute the link budget between two radiating devices by knowing their gain-calibrated spectra. Finally, an alternative approach to evaluate the link budget of antenna measurement systems working at reduced distance has been presented. Such an approach is based on the "NF gain/directivity" definition and it allows a straightforward generalization of the well-known Friis' far field formula.

Acknowledgement

The authors would like to acknowledge J. E. Hansen, who recently passed away, for his precious and inspiring work related to the theory and practice of SNF antenna measurements.

References

[1] J. E. Hansen (ed.), Spherical Near-Field Antenna Measurements, Peter Peregrinus Ltd., on behalf of IEE, London, United Kingdom, 1988

[2] IEEE Std 1720-2012 "Recommended Practice for Near-Field Antenna Measurements"

[3] F. Saccardi, M. A. Saporetti, R. T. Sánchez and L. J. Foged, "Efficient Modelling of Antenna Measurements Including the Impact of the Anechoic Chamber" APS/URSI 2021, 4-10 Dicember 2021, Singapore

[4] F. Saccardi, A. Giacomini, and L. J. Foged "Estimating Antenna Measurements Uncertainty from Quiet Zone Variation" APS/URSI 2023 July 23–28, 2023, Portland, Oregon, USA

[5] Harald T. Friis, "A Note on a Simple Transmission Formula," Proceedings of the I.R.E. and Waves and Electrons, May, 1946, pp 254–256.

[6] R. T. Cutshall, et. all, "Measuring G/T with a Spherical Near-Field Antenna Measurement System via the CW-Ambient Technique," AMTA2020 Newport, RI, USA

[7] F. Saccardi, A. Giacomini, L. J. Foged, "Probe Correction Technique of Arbitrary Order for High Accuracy Spherical Near Field Antenna Measurements", AMTA 2016, Oct. 30 – Nov. 4, Austin, TX, USA

[8] F. Saccardi, A. Giacomini, L. J. Foged, T. Blin "Experimental Validation of Full Probe Correction Technique using Wideband and Dual-Polarized Probes in Spherical NF Antenna Measurements" AMTA 2021, October 24-29, Daytona Beach, FL, USA

[9] Per C. Hansen; F. H. Larsen "Suppression of reflections by directive probes in spherical near-field measurements" IEEE Transactions on Antennas and Propagation, VOL. AP-32, NO. 2, February 1984

[10] IEEE Std 149-2021 "IEEE Recommended Practice for Antenna Measurements"

[11] F. Scattone, D. Sekuljica, A. Giacomini, F. Saccardi, L. J. Foged A. Scannavini, N. Gross, P. O Iversen, "Plane Wave Generator for Direct Far-field Over-The-Air Testing of Devices", AMTA 2018, 4-9 November, Williamsburg, VA, USA